Excited States of 4-Aminobenzonitrile (ABN) and 4-Dimethylaminobenzonitrile (DMABN): Time-resolved Resonance Raman, Transient Absorption, Fluorescence, and ab Initio Calculations†

C. Ma,*,‡ W. M. Kwok,‡ P. Matousek,§ A. W. Parker,§ D. Phillips,‡ W. T. Toner,|| and M. Towrie§

Department of Chemistry, Imperial College, Exhibition Road, London SW7 2AY, UK, Central Laser Facility, CLRC Rutherford Appleton Laboratory, Didcot, Oxfordshire, OX11 0QX, UK, and Department of Physics, Clarendon Laboratory, Parks Road, Oxford, OX1 3PU, UK

Received: July 17, 2001; In Final Form: January 7, 2002

Structures of the locally excited (LE) states of 4-aminobenzonitrile (ABN) and 4-dimethylaminobenzonitrile (DMABN) have been studied by picosecond time-resolved resonance Raman and transient absorption spectroscopy. Contrary to reported time-resolved infrared experiments, our time-resolved resonance Raman spectra show characteristic frequency shifts of several modes from their ground-state values. Combined with ab initio geometric and vibrational analysis of the ground and LE states, our results indicate a similar planar structure for the LE states of both ABN and DMABN. In the LE state, the pyramidal conformation of the ground state flattens along the inversion coordinate, the phenyl ring expands, and the ph-N bond shortens. Partial charge transfer in the LE state, mainly from the amino nitrogen lone pair orbital to the ring π^* orbital, is indicated by the observation of a frequency downshift of the ring CC stretching mode and an $\sim$30 cm^{-1} downshift of the C≡N stretching mode. This is supported by calculated changes of electron distribution in molecular orbitals upon excitation.

1. Introduction

Charge transfer (CT) reactions are of great importance in many fields of chemistry and biology, but many questions remain to be answered. Comparisons of molecules which do not react with analogues that do are useful in resolving issues that depend on subtle structural details, 4-aminobenzonitrile (ABN) and 4-dimethylaminobenzonitrile (DMABN) are such a pair. The electronic donor−acceptor DMABN is a classic case where intramolecular charge transfer (ICT) and structural reorganization take place in polar solvents.[1] This is interpreted as an ICT reaction from a locally excited (LE) to an ICT state that only occurs in polar solvents. Several models[2−5] have been proposed to interpret the nature and structure of the LE and ICT states. At present, only two, TICT (twisted ICT)[2] and PICT (planar ICT),[4] remain under discussion. In the TICT model, the ICT reaction is accompanied by a twisting of the amino group from a conjugated planar configuration in the LE state to an electronically decoupled perpendicular ICT geometry,[2] but in the PICT model, the amino group structure changes from a pyramidalized LE state to a conjugated planar ICT state, and this is supposed to be the rate-determining step for the ICT reaction.[4]

The ICT state has been studied in recent picosecond Kerr gate time-resolved resonance Raman (ps-K-TR^3)[6−8] and time-resolved infrared (TRIR) experiments.[9−11] The observation of an $\sim$96 cm^{-1} downshift of the key ν(ph-N) mode (dominate by phenyl−amino stretching vibration) from its ground-state frequency and the close resemblance of the C≡N stretching and ring local mode frequencies to those of the benzonitrile radical anion[12] strongly favor the TICT model,[13] as does most theoretical work, including calculations of Hynes et al.[14] and Mennucci et al.,[15] in which solvent effects are considered. However, on the basis of systematic measurements of the fluorescence of a wide series of derivatives of DMABN, Zachariasse et al. favor the PICT model.[16] Although no conclusive structural evidence has been reported to support the PICT model and the very recent theoretical work[17] favors the TICT, the PICT model cannot be ruled out.[18,19]

The structure of the DMABN LE state has been investigated by rotationally resolved electronic spectroscopy in the gas phase[20−25] and picosecond time-resolved resonance Raman (ps-TR^3)[6] and TRIR[10] spectroscopy in solution phase. Conflicting results have been presented. Some gas-phase studies suggest the LE state has a 22° or 30° twist between the planes of the amino group and phenyl ring,[20,21,25] but a planar LE structure is suggested by others, as for example, the supercooled molecular jet study of Salgado et al.[22] Solution phase studies are in agreement with the planar structure[6,10] but the key ν(ph-N) mode was not identified. Comparison between the results of our ps-TR^3 measurements and the TRIR study will be discussed in the text below (section 5). Theoretical studies are also in conflict. Ab initio RCIS (Restricted Configuration Interaction Singles) work by Scholes et al.[26] and Lommatzsch et al.[21] supports the twisted conformation, but calculations using CASSCF[13,27] and some other semiempirical methods, with and without solvent effects, lend support to a planar geometry.[28−30] Recently, the possibility of a slightly wagged LE conformation has also been suggested.[13,27]

In contrast to DMABN, ABN does not undergo the ICT reaction in either the gas or solution phase and only normal

† Part of the special issue "MitsuoTasumi Festschrift".
* Corresponding author. E-mail: c.ma@ic.ac.uk
‡ Imperial College.
§ Central Laser Facility, CLRC Rutherford Appleton Laboratory.
|| Clarendon Laboratory.

10.1021/jp012765e CCC: $22.00
Published on Web 03/09/2002

fluorescence can be observed, even in polar solvents.[16,21] The absence of the ICT fluorescence in ABN has been attributed to an increased energy gap between the two lowest excited states and a lower amino group donor strength.[16] It has often been taken as a model for the LE state of DMABN.[10,13,16,21,23,27,29,31,32] From gas phase rotationally resolved excitation spectroscopy studies, pyramidal or planar structure has been suggested.[21,23,33−36] Based on a comparison of the experimental TRIR spectrum with CASSCF calculations, Chudoba et al.[10] and Dreyer et al.[13,27] proposed a conformation with a pyramidal amino group. However, this view contradicts theoretical work predicting a planar structure for the S_1 state of ABN.[21]

To clarify and establish the structural and electronic properties of the LE states of DMABN and ABN, we obtained ps-K-TR^3 spectra over the 800−2400 cm^{-1} range. Spectra of methyl-deuterated DMABN (DMABN-d_6) were used to help assign modes related to the dimethylamino group. To find suitable TR^3 probe wavelengths for the TR^3 experiments and also to help identify the intermediate species probed, the transient absorption (TA) of ABN and DMABN was measured. To relate the experimental observations to excited-state structure, equilibrium geometries and vibrational frequencies were calculated by the ab initio RCIS method.

The ground-state structures of ABN and DMABN have been determined by X-ray diffraction analysis (crystalline)[37] and microwave spectroscopy (gas phase).[20] The LE state frequency shifts from ground-state values of modes such as the C≡N stretch and ν(ph-N), not hitherto determined, are sensitive to extent of the ICT and amino group conformation, respectively, requiring accurate information on ground-state vibrational spectra. Vibrational spectra and analyses of ground-state DMABN based on density function theoretical (DFT) ab initio calculation and isotopic shifts observed in various DMABN isotopomers have recently been reported by Okamoto et al.[38] and ourselves.[39] Assignments of several modes, such as ν(ph-N) and ν(ph-CN), which are sensitive to structure, differ from those reported by Gates et al.[40] and Schneider et al.[41] on the basis of empirical and semiempirical force field methods, respectively. We conclude that, when using a reasonable description of the electronic interaction between N lone pair and the ring π system in DMABN (strong nπ-conjugation), the quantum chemical force field of the DFT method is superior to the empirical and semiempirical ones in predicting vibrational modes.[38,39] Empirical and semiempirical vibrational analyses of ABN have been reported by Kumar et al.[42,43] and Schneider et al.,[41] respectively. These give conflicting assignments for many bands, including ν(ph-N). We therefore made DFT calculations of IR and Raman spectra of the ground state of ABN. As expected, the calculations reproduce the experimental spectra satisfactorily and the results suggest revised attributions for many important bands.

This paper is arranged as follows: after a brief description of experimental and computational methods, we present a vibrational analysis of the ground state of ABN. We then present and discuss fluorescence, transient absorption, and time-resolved resonance Raman spectra of the LE states of ABN and DMABN. Finally, we compare the observed excited-state frequencies with values calculated using the RCIS method. Our experimental and calculated ground/LE frequency shifts and optimized excited-state structures provide strong evidence that ABN and DMABN have similar planar LE state structures. This clarifies the controversy on these states and is also helpful in understanding the ICT mechanism of dual fluorescence compounds.

2. Experimental Section

ABN and DMABN samples from suppliers were recrystallized from hexane three times before use. DMABN-d_6 was synthesized according to the method given in ref 3 and its purity confirmed by NMR and mass spectroscopic analysis. Spectroscopic grade solvents were used as received. The normal Raman spectrum of ABN was measured in the solid phase with 628 nm excitation using an ISA Infinity Raman system. The depolarization ratio (ρ) was calculated from the parallel-to-perpendicular ratio of the integrated areas of bands recorded in acetonitrile solution. The IR spectrum of ABN in solid KBr was recorded using a Perkin Elmer FT-IR spectrometer 1760X. The resolution of both the Raman and IR spectra was 1 cm^{-1}. The steady-state fluorescence spectra of ABN and DMABN were measured using a SPEX FluoroMax spectrometer.

Time-resolved experiments were carried out using a system[44,45] based on optical parametric amplifiers (OPAs). Transient absorbance spectra were measured under "magic angle" conditions using the arrangement described in ref 6, with a pump wavelength of 267 nm. The ps-K-TR^3 spectra of the LE states of ABN and DMABN were obtained using the methods described in refs 6, 7, and 8, with pump and probe wavelengths of 267 and 460 nm, respectively. TR^3 spectra of the LE state of DMABN and DMABN-d_6 were obtained with 267/600 nm pump/probe wavelengths. Each spectrum shown is the sum of three individual background-subtracted spectra with accumulation times typically of 2000 seconds. The spectra were not corrected for variations in spectral throughput and detector efficiency.

Acetonitrile Raman bands were used to calibrate the spectra with an estimated accuracy in absolute frequency of ±10 cm^{-1}. Sample concentrations were $1-5 \times 10^{-3}$ mol dm^{-3}. UV absorption measurements before and after sample use revealed no degradation.

3. Calculation

Ab initio calculations were made using Gaussian 98.[46] Restricted Hartree−Fock (HF) and DFT calculations with 6-31G(d) and cc-pVDZ basis sets were made to obtain optimized geometry and vibrational frequencies of ground-state ABN and Raman and IR activities. The DFT calculation was performed with Becke's three-parameter hybrid method using the Lee−Yang−Parr correlation functional (B3LYP). According to experimental data,[37] C_s symmetry was assumed for the ground state.

Calculations of excited-state ABN and DMABN were made using RCIS with 6-31G(d) and cc-pVDZ basis sets for ABN and 6-31G(d) for DMABN. To determine the true minima on the LE state potential surface, various initial geometries of different symmetry were explored, such as C_1, C_s, and C_{2v}. RCIS calculations usually overestimate excitation energy and are not adequate for computing one-electron properties of excited states due to neglect of dynamical electronic correlations. However, accurate geometries have been predicted for many molecules.[21,47] It will be seen below that the results provide a qualitatively reasonable interpretation to the experimental observations.

Assignments of the calculated modes were made according to calculated atomic displacements of the corresponding vibrations. Wilson notation was used to label the ring CC and CH vibrations analogous to benzene motions. We assigned the observed vibrational bands by comparing the calculated and experimental frequencies. For the ABN ground-state modes, the attributions were also based on comparison of the calculated

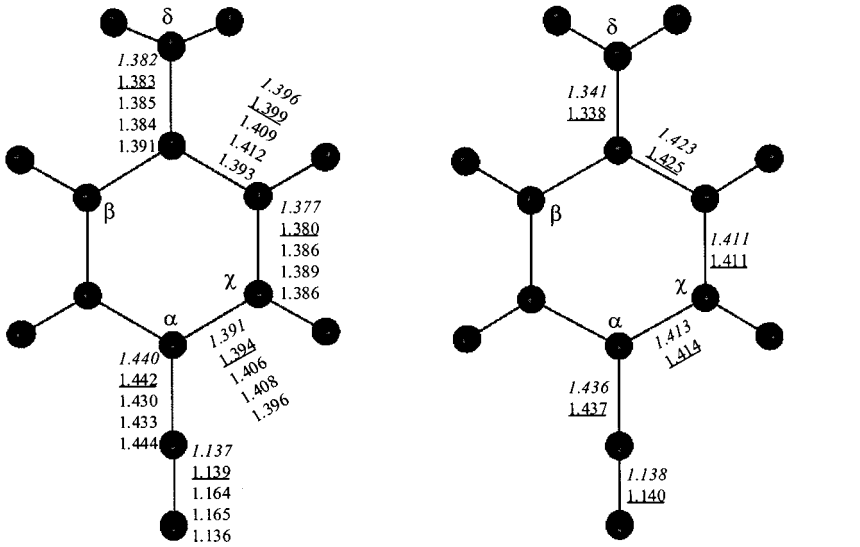

	α	β	χ	δ	Inversion
HF/6-31G(d)	*119.1*	*120.5*	*120.6*	*112.3*	*36.0*
HF/cc-pVDZ	119.0	120.5	120.6	111.7	38.4
DFT/6-31G(d)	118.8	120.7	120.6	112.9	33.5
DFT/cc-pVDZ	118.7	120.8	120.7	112.8	34.0
Experiment[a]					34(3)

	α	β	χ	δ	Inversion
RCIS/6-31G(d)	*122.2*	*118.9*	*119.1*	*117.5*	*0.0*
RCIS/cc-pVDZ	122.4	118.9	119.0	117.9	0.0

Ground state **LE state**

Figure 1. Optimized structural parameters of the ground and LE state of ABN using different methods and basis sets. Bond distances are in Å and bond angles in degrees. [a] Reference 37.

TABLE 1: Calculated Energies (in Hartree) and Dipole Moments (in Debye) of the Ground State of ABN Using Different Methods and Basis Sets

method	HF		DFT		expt
basis set	6-31G(d)	cc-pVDZ	6-31G(d)	cc-pVDZ	
symmetry	C_s: A′	C_s: A′	C_s: A′	C_s: A′	C_s[a]
energy (Hartree)	−377.46986	−377.50358	−379.849	−379.87591	
dipole moment (D)	6.5	6.5	6.7	6.7	6.6[b]

[a] Reference 37. [b] Reference 3, in cyclohexane.

and observed Raman and IR activities as well as the depolarization ratios of Raman bands.

4. Results

4.1. Vibrational Analysis of the Ground State of ABN. Geometric parameters of the optimized structure of ground-state ABN using HF and DFT methods with different basis sets are presented in Figure 1. Experimental values[37] are displayed for comparison. Calculated total energies and dipole moments are collected in Table 1. Similar results are obtained from all computations, and the calculated structures are in good agreement with experiment. The ground state of ABN was found experimentally to have a pyramidal amino group with the N atom being opposed to the H atoms and ∼0.005 Å out of the plane of the phenyl ring.[37] This structure was reproduced fairly well by the computations. The inversion angle calculated at the DFT/cc-pVDZ level reproduces the experimental value of 34° (Figure 1). The dipole moments of the ground state of ABN calculated in HF and DFT of 6.5 and 6.7 D, respectively, also correlate well with the experimental value of 6.6 D.[3]

The larger of the two basis sets used, cc-pVDZ, is expected to be more reliable for computing one-electron properties than is the 6-31G(d) basis set, and it can be seen from Table 1 that it produces lower total energies than the 6-31G(d) at both HF and DFT levels. However, the 6-31G(d) and cc-pVDZ optimized geometries and dipole moments are very similar at both levels. This implies that 6-31G(d) is reliable enough for the interpretation of experimental data for molecules of the ABN type. This is also confirmed by the vibrational analysis below.

Figure 2 displays experimental and calculated (DFT/6-31G-(d)) Raman and infrared spectra of ground-state ABN from 300 to 1700 cm^{-1}. Calculated frequencies were scaled by a factor of 0.9629 to minimize the root-mean-square difference between calculated and experimental values for bands having definite identifications, very close to the recommended value of 0.9613.[38] Calculated Raman and IR activities are shown without modification, and calculated bands are represented by Lorentzians with a width of 10 cm^{-1}. Rauhut et al.[48] have demonstrated that DFT with the B3LYP functional and 6-31G(d) basis set, as used here, is a reliable tool for the calculation of the vibrational force field and interpretation of vibrational spectra and predicts frequencies and intensities better than RHF. This is indeed observed in our computations. Among the four methods, DFT/6-31G(d) reproduces the data best.

It is clear from Figure 2 that the principal features of the observed Raman and IR spectra are reproduced satisfactorily by the calculation. This allows direct attribution of experimental bands from comparison of calculated and observed spectra and calculated symmetry and measured depolarization ratios of Raman bands. Assignments of most bands with frequency above 600 cm^{-1} are affirmative due to the accurate simulation in this region. Deviations between calculation and experiment can be

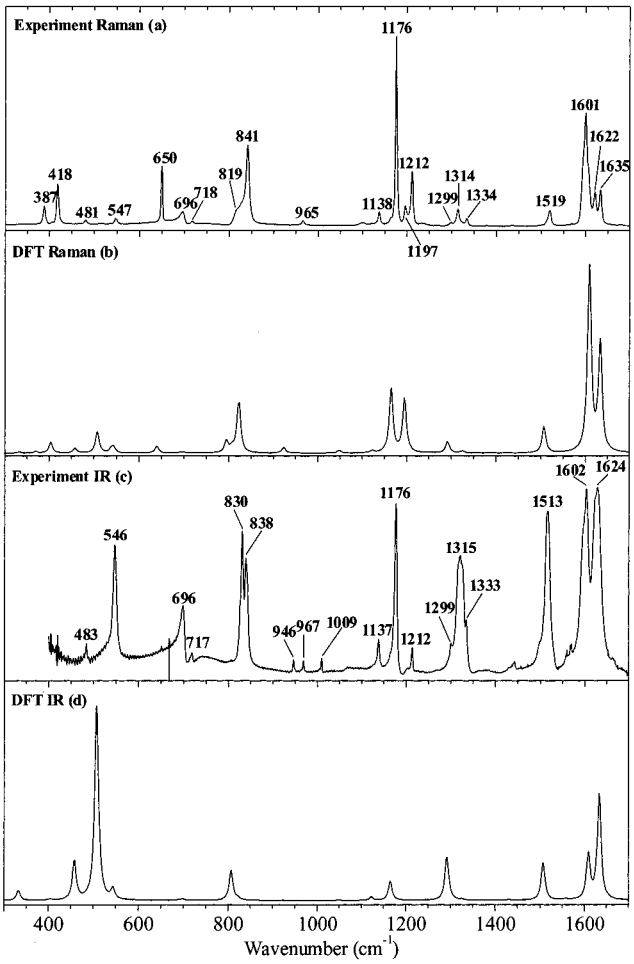

Figure 2. Experimental and DFT calculated normal Raman (a) and (b) and IR (c) and (d) spectra in the 300−1700 cm^{-1} region for ABN in the ground state. (No IR measurement was made below 400 cm^{-1}.)

found for low-frequency bands below 600 cm^{-1}, and assignments in this region are tentative. Table 2 summarizes the observed Raman and infrared frequencies, Raman depolarization ratios, calculated frequencies, symmetries, and approximate descriptions of the calculated normal modes. As most of the Raman bands observed in the LE state spectrum of ABN (Figure 5a) appear in the 1100−2400 cm^{-1} region, only those ground-state bands that fall in this range will be discussed.

We assign the C≡N stretching, NH_2 symmetric scissoring and several ring local CC stretching modes, dominated and described approximately by the Wilson 8a, 8b, 19a, and 19b to bands observed at 2211, 1622, 1601, 1567, 1519, and 1436 cm^{-1}, in agreement with previous attributions.[41,42] The broad band previously observed at 1630 cm^{-1} was resolved as composed of two bands at 1635 and 1622 cm^{-1} in the present work (Figure 2a). As no calculated fundamental can be found corresponding to 1635 cm^{-1}, it may be a combination band or overtone. This is also the case for a weak band at 1197 cm^{-1} (Figure 2a).

Our other assignments, discussed below, differ substantially from the work of Schneider et al.[41] and Kumar et al.,[42] especially in the crowded 1100−1350 cm^{-1} spectral range and including vibrations such as ν(ph-N), which are particularly relevant to structural change. We believe that the present calculations, made at a significantly higher level should be more reliable.

The strong infrared band at 1315 cm^{-1} is reproduced accurately by the calculation (Figure 2), and can be attributed confidently to a mode dominated by the ν(ph-N) stretch. Two shoulders (at 1334 and 1299 cm^{-1}) are assigned to the ring asymmetric Wilson 14 (CC stretching) and 3 (CH in plane bending) modes, respectively. The former corresponds to a weak but clearly resolved band at 1334 cm^{-1} in our Raman spectrum (Figure 2a), not previously reported. Our attribution of the observed 1315 cm^{-1} band is supported by CASSCF calculations by Chudoba et al.,[10] but Schneider et al.[41] assigned it to Wilson 14 and Kumar et al.[42] to Wilson 3.

Attribution of the bands observed at 1212 and 1176 cm^{-1} (Figure 2a, 2c) to modes dominated by ν(ph-CN) and Wilson 9a (ring CH in plane bending), respectively, is also straightforward based on a good match with the DFT calculation and depolarization ratios. Our assignment of the 1212 cm^{-1} band is consistent with Schneider et al.[41] However, both Kumar et al.[42] and Schneider et al.[41] attributed the 9a mode to a band at 1140 cm^{-1}, seen at 1138 cm^{-1} in this work, which we attribute with certainty to another ring CH in-plane bending mode, Wilson 18b, as indicated by the calculation.

The key modes of ground-state ABN relevant to excited-state properties are the C≡N stretching, Wilson 8a, 19a, and ν(ph-N) modes, which we have attributed to the bands observed at 2211, 1601, 1519, and 1314 cm^{-1}. The corresponding DMABN ground-state bands lie at 2210, 1600, 1523, and 1369 cm^{-1}.[38,39] As deduced from the X-ray analysis,[37] the major ground-state structural difference between ABN and DMABN is related to amino group conformation: the respective inversion angles are 34° and 11°, and the ph-N bond lengths are 1.391 and 1.377 Å. This is consistent with only the ν(ph-N) vibration showing a significant difference in frequency due to the more pyramidal character of ABN than DMABN in the ground state. It also correlates well with similar vibrations in closely related amino benzene compounds. For example, ν(ph-N) is recorded at 1348 and 1278 cm^{-1} for the ground states of dimethylaniline (DMA)[49,50] and aniline,[48] respectively, whose inversion angles are measured to be 27° and 37−40°, respectively.[51−54] DMABN and DMA have less pyramidalization character than do ABN and aniline due to the $-N(CH_3)_2$ group having donor strength greater than that of the $-NH_2$ group. The existence of an electron acceptor group in the para position, the cyano group in this case, reduces further the pyramidal character, as can be seen from comparisons of DMA with DMABN and aniline with ABN.

The ν(ph-N) frequency is useful in evaluating the bonding conformation of the amino group and the electron distribution in aromatic amine compounds. A frequency decrease from DMABN to DMA to ABN to aniline is an indication of decrease in bond order thus increase of the ph-N bond length, which is also linked to a decrease in the extent of nπ conjugation and to an increase in the amino group inversion from ∼11° to ∼40° across the set. Studies of geometrical parameters in a series of para-substituted anilines[55,56] show that the ph-N bond length increases linearly with the inversion angle. However, as found from the vibrational analysis of ABN and DMABN, the vibration dominated by the ν(ph-N) is a complex mode with additional contributions from the ring modes 19a (CC stretching), 18a (CH in-plane bending), and a methyl deformation motion, and the coupling is much stronger in DMABN[38,39] than in ABN. This makes it hard to predict the amino conformation of the excited state merely from the frequency shift of this mode, because the shift could also be due to changes of other structural parameters normally observed for aromatic compounds upon photoexcitation, such as the ring C−C lengths. A full comparison between the experimental and calculated frequencies of the LE state is therefore necessary to determine the structure.

TABLE 2: Observed and DFT Calculated Vibrational Frequencies (cm^{-1}) and Assignments of ABN in the Ground State (C_s Point Group)

observation			calculation		
IR	Raman	ρ	symmetry	DFT	assignment
	342		A″	332	NH_2 rocking, 18b (ring CH in-plane bending)
	387	*a*	A″	369	ph-N in-plane bending
			A″	399	16a (ring CC out-of-plane def.)
	418	0.3	A′	403	6a (ring CC in-plane def.)
483	481	0.3	A′	458	NH_2 wagging
546	547	?	A′	508	NH_2 wagging
			A″	539	ph-N in-plane bending, 6b
			A′	544	16b (ring CC and CH out-of-plane def.)
	650	*a*	A″	640	6b (ring CC in-plane def.)
696	696	<0.1	A′	691	12 (ring CC in-plane def.)
717	718	?	A′	700	4 (ring out-of-plane def.)
	819	?	A″	794	10a (ring CH out-of-plane bending)
830	819	?	A′	807	17b (ring CH out-of-plane bending)
838	841	0.2	A′	822	1 (ring breathing)
946			A″	917	10b (ring CH out-of-plane bending)
967	965	?	A′	924	17a (ring CH out-of-plane bending)
1009			A′	993	18a (ring CH in-plane bending)
	1100	?	A″	1048	NH_2 rocking, 18b (ring CH in-plane bending)
1137	1138	?	A″	1123	18b (ring CH in-plane bending)
1176	1176	0.3	A′	1165	9a (ring CH in-plane bending)
1212	1212	0.3	A′	1195	ν(ph-CN)
1299	1299	?	A″	1290	3 (ring CH in-plane bending)
1315	1314	<0.1	A′	1292	ν(ph-N)
1333	1334	?	A″	1325	14 (ring CC stretching)
	1436	?	A″	1430	19b (ring CC stretching)
1513	1519	0.3	A′	1507	19a (ring CC stretching)
1567		?	A″	1558	8b (ring CC stretching)
1602	1601	0.4	A′	1609	8a (ring CC stretching)
1624	1622	0.4	A′	1634	NH_2 scissoring
2212	2211	0.2	A′	2252	C≡N

[a] Depolarized band, ? represents weak features with uncertain ρ value.

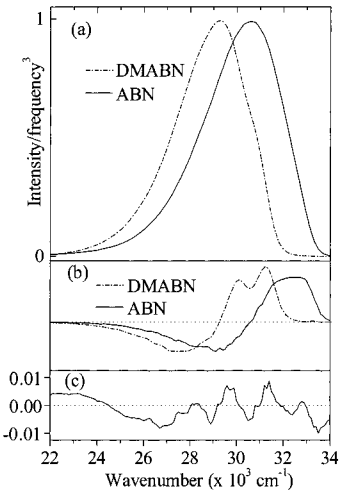

Figure 3. Fluorescence of ABN and DMABN. (a) Fluorescence spectra in hexane in vibronic units (intensity/frequency^3 vs frequency); (b) derivatives of spectra in (a) with respect to frequency (arbitrary scale); (c) difference between ABN data in (a) and model spectrum derived from DMABN data in (a) as described in the text, relative to peak intensity of (a).

4.2. LE State Spectra. Figure 3a shows fluorescence spectra of ABN and DMABN in hexane and Figure 3b shows their derivatives with respect to frequency. Vibronic units (intensity/frequency^3 vs frequency) are used. The spectra are very similar but the structure on the rising edge of the DMABN spectrum, seen very clearly in the derivative, is absent in ABN.

If the DMABN data are convolved with a Gaussian to simulate increased solvent broadening, the result does not match the ABN profile, indicating a real difference in the structure of the vibronic spectrum. This spectral difference can be quantified as follows. We recall that convolution can be used in ab initio spectral simulations to fold in the contribution of a mode or group of modes that is not mixed with the remainder.[57] Differences from a reference data spectrum due to increases in optical activity can therefore be simulated by convolving the data with the stick spectrum of a suitable model satisfying this condition. Decreases in activity are modeled by deconvolution (see Appendix). The model can include anharmonic modes and mixing within, but not between, the convolved, deconvolved, and remainder groups. Solvent broadening and all other properties of the reference spectrum are unchanged. It is assumed this method will provide a first approximation when comparing spectra of unknown composition, mixing, and anharmonicity, enabling small spectral differences to be quantified using a few explicit assumptions. For simplicity, the harmonic approximation for modes without frequency change is used to compute the intensities of the model fundamentals and overtones, I_n:

$$I_n = (s^n/n!)\exp(-s) \qquad (1)$$

where s is half the square of the normalized displacement and $n = 1$ denotes the fundamental. The model "convolution difference spectrum" that fits the data can easily be calculated using the parameters given below.

The convolution of the DMABN data with the stick spectrum of a mode with frequency between 400 and 500 cm^{-1} and $s \sim 0.5$ to 1.1 is sufficient to match the ABN spectrum from 34000 to 29000 cm^{-1} at the 1% level. The whole ABN spectrum can be reproduced with residuals ~0.4% of the peak by convolving the DMABN data with stick spectra of modes at 500 ($s = 0.77$) and 2200 ($s = 0.14$), and deconvolving at 1400 ($s = 0.2$). The residuals are shown in Figure 3c. This quantifies the differences

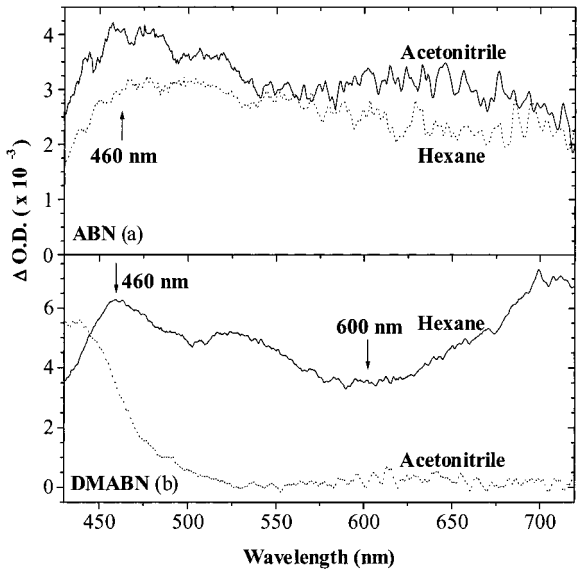

Figure 4. Transient absorption spectra of ABN (a) and DMABN (b) in hexane and acetonitrile with excitation at 267 nm, at 50 ps delay time.

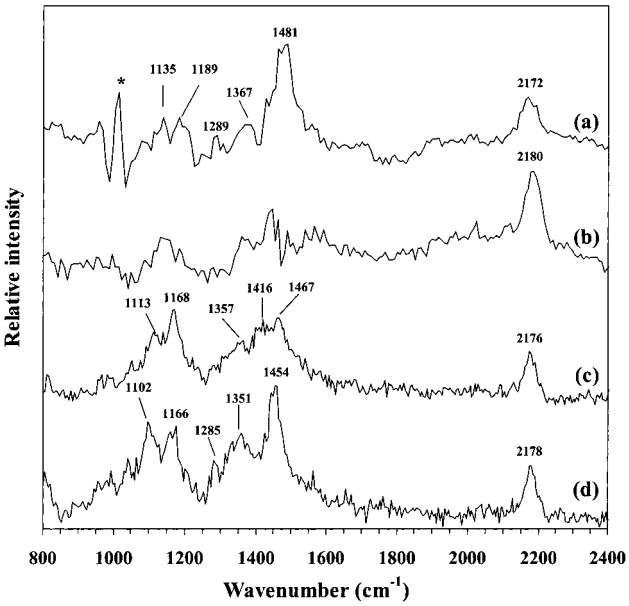

Figure 5. Picosecond Kerr-gated time-resolved resonance Raman spectra of ABN in methanol (a) and DMABN in hexane (b) with 267 nm pump and 460 nm probe wavelength at 50 ps delay time. Picosecond time-resolved resonance Raman spectra of DMABN (c) and DMABN-d_6 (d) in cyclohexane with 267 nm pump and 600 nm probe wavelength at 50 ps delay time. The asterisk indicates improper solvent band subtraction.

between the spectra to the estimated systematic accuracy of the data without any change in solvent broadening. Resolution is too limited to say whether the changes are due to modes that are active in both molecules, or only one. Poorer but acceptable fits can be obtained using smaller activity at 500 (*s* down to ~0.4) plus Gaussian broadening with up to ~250 cm^{-1} standard deviation. Since the actual physical differences may well involve mixed or anharmonic modes, perhaps with barriers, all that can be said with certainty is that the spectral differences are largely due to molecular differences rather than solvent broadening and that activity at ~500 cm^{-1} is significantly enhanced in ABN, to the approximate degree indicated by the model. Other differences are small but nonzero. The enhancement at ~500 cm^{-1} may relate to the larger ABN ground-state inversion angle if both molecules are planar in LE, and we note that modes associated with the amino group in ABN are found in the 450 to 550 cm^{-1} region (Table 2). Limited experimental resolution precludes a definite assignment.

Transient absorption spectra of ABN and DMABN in hexane and acetonitrile, excited at 267 nm, are shown in Figure 4. The fine structure is due to uncorrected instrumental effects. The ABN spectra (Figure 4a) resemble the spectrum of DMABN in nonpolar hexane (Figure 4b) and change little with time. There is no significant solvent dependence for ABN, in contrast to the well-known behavior of DMABN,[58] where there is no ICT reaction in nonpolar solvent but an isobestic point at ~455 nm indicates the picosecond time scale transfer from LE to ICT in acetonitrile.[59] These observations are in good agreement with the scenario that LE states of similar properties are formed in ABN in either polar or nonpolar solvent and in DMABN in nonpolar solvent.

The ps-K-TR^3 experiments were carried out for ABN and DMABN with pump and probe wavelengths of 267 and 460 nm, respectively, as well as ps-TR^3 measurements of DMABN and DMABN-d_6 at 600 nm probe wavelength where the Kerr gate was not required. The probe wavelengths used are indicated by arrows in Figure 4. The pump wavelength falls into the lowest absorption band of ABN and DMABN. The spectra obtained are shown in Figure 5.

The DMABN spectrum at 600 nm probe wavelength (c) is very similar to that previously obtained in cyclohexane using a 615 nm probe.[6] The spectrum of DMABN-d_6 in nonpolar solvent (d) has not been reported previously. Bands appearing between ~1000 and 1600 cm^{-1} are not well resolved in the 460 nm DMABN spectrum (b), but the C≡N stretch at 2180 cm^{-1} is clearly seen and we note that it is absent in polar solvents at 400 nm probe wavelength but has been observed at 2095 cm^{-1} using 330 nm probe wavelength at 50 ps delay.[7] Interference effects may occur in resonance Raman scattering when the absorption bands of electronic states overlap,[60] as is likely to be the case here. There may also be mode mixing. In the absence of Raman excitation profiles, band intensities therefore give only a qualitative indication of molecular properties and no definite conclusions can be drawn, but we take the data to indicate that S_n states of similar character are resonant with LE at both 460 and 600 nm (or there is a single very broad state in this region). The spectrum of ABN in methanol at 460 nm probe wavelength (a) closely resembles the 600 nm spectrum of DMABN in hexane (c), indicating that both molecules have LE and S_n states of similar character and ABN does not form the ICT state in polar solvent.

Band positions and relative intensities obtained using unconstrained Lorentzian fits are summarized in Table 3. Tentative assignments, RCIS calculated frequencies (scaled by 0.8923), and frequencies of the corresponding bands in the ground states are included in the table for comparison. The assignments are based on DMABN/DMABN-d_6 isotopic shifts for DMABN and the RCIS frequency calculations for both ABN and DMABN.

It is important to note that all the spectra in Figure 5 show the C≡N stretch at ~2180 cm^{-1}, corresponding to the same ~30 cm^{-1} downshift for ABN and DMABN relative to the ground state. This indicates a decrease of the C≡N bonding order and can be interpreted as being due to a similar degree of partial localization of transferred charge on the cyano antibonding orbital in the LE states of both molecules. (Full transfer and localization is indicated by a ~175 cm^{-1} downshift of the C≡N stretching in the triplet state of DMABN,[61] while in the ICT state of DMABN, a ~115 cm^{-1} downshift, corresponds to

TABLE 3: Observed and RCIS Calculated Raman Band Frequencies and Their Assignments for the LE States of ABN, DMABN, and DMABN-d_6 (observed ground state frequencies included for comparison)

	LE state							S_0 state		
	ABN			DMABN		DMABN-d_6		ABN	DMABN	DMABN-d_6
assignment	expt	cc-pVDZ	6-31G(d)	expt	6-31G(d)	expt	6-31G(d)	expt	expt[a]	expt[a]
C≡N	2172 (1.0)	2288	2299	2176 (1.0)	2294	2178 (1.0)	2294	2211	2210	2210
19a (ring CC streching)	1481 (1.5)	1437	1446	1467 (1.4)	1477	1454 (3.2)	1466	1519	1523	1515
δ_{Me} (methyl deformation)				1416 (1.1)	1420		1122		1414	1134
ν(ph-N)	1367 (0.4)	1295	1297	1357 (0.6)	1357	1351 (2.4)	1360	1314	1370	1375
3 (ring CH bending)	1289 (0.2)[b]	1272	1288	1325 (0.3)[b]	1308	1285 (0.2)[b]	1309	1299	1306	1306
ν(ph-CN), 9a (ring CH bending)	1189 (0.6)	1141	1143	1168 (1.5)	1154	1166 (1.5)	1166	1212	1227	1227
9a (ring CH bending), ν(ph-CN)	1135 (0.6)	1109	1124	1113 (1.0)	1136	1102 (2.0)	1142	1176	1180	1178

[a] References 38 and 39. [b] Weak features of uncertain assignment.

TABLE 4: Calculated Energies (in Hartree), Dipole Moments (in Debye), Excitation Energies (in cm^{-1}), and Oscillation Strengths of the LE States of ABN and DMABN Using the RCIS Method with Different Basis Sets

	ABN			DMABN	
method	RCIS		expt	RCIS	expt
basis set	cc-pVDZ	6-31G(d)		6-31G(d)	
symmetry	C_s: A″	C_s: A″		C_s: A″	
energy (Hartree)	−377.49588	−377.45893		−455.51474	
dipole moment (D)	7.8	7.9	8.0[a]	8.8	9.9[a]
excitation energy (cm^{-1})	43997	46788	33842[c]	45057	32247[b]
oscillation factor	0.0624	0.0539	very weak	0.0502	very weak
transition moment	short axis	short axis	short axis[c]	short axis	short axis[b]

[a] Reference 3, in cyclohexane. [b] Reference 22. [c] Reference 23.

full charge transfer but delocalization over the benzonitrile subgroup.[7−10])

The other striking aspect of Figure 5 is that the strong band at 1481 cm^{-1} in the ABN spectrum and the features at 1367, 1189, and 1135 cm^{-1} all have slightly downshifted counterparts in the DMABN and DMABN-d_6 spectra recorded at 600 nm probe wavelength. Comparing DMABN (Figure 5c) with DMABN-d_6 (Figure 5d), it can be seen that all the bands are insensitive to methyl group deuteration, except for one unresolved feature at 1416 cm^{-1} in DMABN. The ring CC stretching and some CH in-plane bending and ring-substituent stretching vibrations of normal substituted aromatic compounds are expected to appear in this region.[62] According to the RCIS result (see below) and also with reference to the established ground state vibrational assignments and corresponding modes of closely related compounds,[49,50,63] the observed common bands were tentatively attributed to totally symmetric vibrations dominated by the Wilson 19a (ring CC stretching), ν(ph-N), ν(ph-CN), and Wilson 9a (ring CH in-plane bending) modes (Table 3). Being sensitive to methyl group deuteration, the 1416 cm^{-1} band can readily be attributed to a methyl deformation mode that may correspond to the 1448 cm^{-1} band in ground-state DMABN.[38,39] This is consistent with the absence of this band in the spectrum of ABN (Figure 5a) and the calculated result.

Most of the recorded bands in the LE states of both ABN and DMABN were observed at frequencies shifted from ground-state values. Besides the C≡N stretch, for example, the ABN mode dominated by Wilson 19a has ∼37 cm^{-1} downshift while the band dominated by ν(ph-N) upshifts by ∼53 cm^{-1} from the ground to LE state. We note that these frequency shifts observed using TR^3 in this and our previous work[6] are not seen in the TRIR experiments.[10] This experimental contradiction is discussed further in section 5.

We conclude that the experimental fluorescence, transient absorption and TR^3 spectra of the LE states of ABN and DMABN are very similar, indicating similar electronic and vibrational properties.

4.3. Ab Initio Calculations of the LE States of ABN and DMABN. The ABN calculation was carried out with both the 6-31G(d) and cc-pVDZ basis sets. Pyramidal as well as planar structures (inversion angle = 0°) were found in our geometry optimization of the LE state, but short-axis polarization was found only for the optimized planar LE state. Since gas-phase rotationally resolved fluorescence experiments[21−23,33] and solution phase[64] anisotropy measurements establish that the LE states of both ABN and DMABN arise from weakly allowed L_b type $S_1 \leftarrow S_0$ transitions with short-axis polarization, we take the optimized planar structure to be the LE state conformation. The LE state calculation of DMABN using 6-31G(d) resulted in a planar optimized structure with transition moment oriented along the short axis of the molecule (the cc-pVDZ calculations failed to converge). Although the optimized geometries actually have C_{2v} symmetry, C_s was assumed for all computations, for comparison with ground-state calculations. Frequency analysis of the optimized planar structure of ABN using cc-pVDZ gave positive values for all modes, but using 6-31G(d), one ABN and two DMABN low-frequency modes of A″ symmetry had imaginary values. This may be due to deficiencies of the RCIS method when used with this basis set or to the crude level of calculation.[21] We note that similar LE geometries have been predicted for both molecules by the CASSCF method.[13,27]

Structural parameters of the LE state of ABN and DMABN obtained by geometry optimizations are displayed in Figure 1 and Figure 6, respectively. For comparison, HF and DFT, 6-31G(d), parameters for ground-state DMABN[39] are also given in Figure 6. It can be seen from the results summarized in Table 4 that calculated transition and dipole moments correlate well with experiment but excitation energies are overestimated.

From Figures 1 and 6, it is clear that calculated structural differences from the ground state predicted for the LE states of ABN and DMABN are similar. Comparing LE-state RCIS and ground-state HF calculations made with the same basis sets (values in italic format for 6-31G(d) and with underline for cc-pVDZ), the pyramidal amino groups are flatter in the LE states of both ABN and DMABN than in the ground states, the phenyl

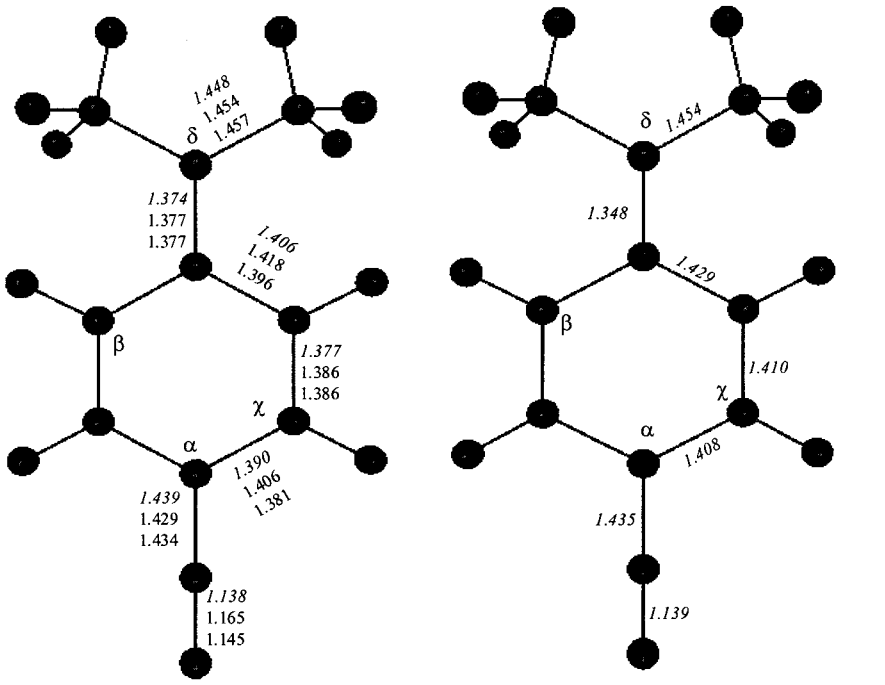

	α	β	χ	δ	Inversion
HF/6-31G(d)[a]	*118.5*	*121.0*	*121.0*	*118.4*	*15.2*
DFT/6-31G(d)[a]	118.4	121.1	121.0	119.7	1.0
Experiment[b]				116.5	10.8

	α	β	χ	δ	Inversion
RCIS/6-31G(d)	*121.5*	*119.8*	*119.6*	*118.3*	*0.0*

Ground state **LE state**

Figure 6. Optimized structural parameters of the ground and LE state of DMABN using different methods with 6-31G(d) basis sets. Bond distances are in Å and bond angles in degrees. [a] Reference 39. [b] Reference 37.

TABLE 5: Experimental and Calculated Frequency Shifts of Observed Raman Bands on Going from the Ground to LE States of ABN, DMABN, and DMABN-d_6

	ABN			DMABN		DMABN-d_6	
	expt	cc-pVDZ	6-31G(d)	expt	6-31G(d)	expt	6-31G(d)
C≡N	−39	−17	−15	−34	−18	−32	−18
19a (ring CC stretching)	−38	−54	−61	−56	−39	−61	−44
δ_{Me} (methyl deformation)				2	5		
ν(ph-N)	53	37	32	−13	14	−24	31
3 (ring CH bending)	−10	−14	−23	19	42	−21	−9
ν(ph-CN), 9a (ring CH bending)	−23	−27	−35	−59	−34	−61	−35
9a (ring CH bending), ν(ph-CN)	−41	−28	−29	−67	3	−76	−15

rings are larger (CC bonds increase by ∼0.020−0.035 Å for both ABN and DMABN), the ph-N bond contracts (∼0.04 Å for ABN, ∼0.026 Å for DMABN), the ph-CN bond is slightly shorter (∼0.004 Å for ABN and DMABN) and there is a very small change of C≡N bond length (increase by ∼0.001 Å for ABN and DMABN).

To evaluate the reliability of the calculated results and relate them to experimental observations, it is worthwhile to compare the experimental frequency shifts on going from the ground to LE state with the calculated ones. Table 5 lists calculated and experimental ground/LE frequency changes for bands observed in the ps-TR[3] spectra (Figure 5) of ABN, DMABN and DMABN-d_6. The calculated values were obtained by subtracting ground-state HF frequencies from the corresponding LE state RCIS frequencies computed using the same basis set.

It can be seen from Table 5 that agreement between the experimental and calculated results is fairly good for ABN. For example, the downshift of the ABN C≡N stretch and ring modes 19a and 9a and upshift of the ν(ph-N) stretch are all predicted reasonably well by the computation. We therefore suggest a planar structure for the ABN LE state. It is interesting to note that the ∼53 cm^{-1} upshift (Table 5) of the ABN ν(ph-N) frequency on going from the ground (1314 cm^{-1}) to the LE state (1367 cm^{-1}) might be a direct indication of enhanced nπ conjugation in the LE compared with ground state, which leads to shortening of the ph-N bond and, quite possibly, flattening of the amino group. The downshift of the ring CC stretching mode (19a, Table 5) from its ground-state frequency implies reduced ring π bonding density, which can also be attributed to occupation of the ring antibonding π^* orbital upon excitation and is consistent with the enlargement of the ring skeleton indicated by the RCIS structural calculation. We note that this is consistent with the geometric change of the analogous aniline molecule in photoexcitation.[65,66] Extensive studies have shown that the $S_1 \leftarrow S_0$ excitation of aniline flattens the molecule from a pyramidal (S_0) to quasiplanar (S_1) geometry along the inversion coordinate, expands the phenyl ring and shortens the ph-N bond.[65−67] It is expected that the cyano electron acceptor group at the para-amino position will enhance a similar geometric change in both ABN and DMABN.

The agreement with experiment is less good for some modes of DMABN. The major inconsistency is that the ν(ph-N) mode is calculated to shift up by 14 cm^{-1} on going from the ground to LE state, but experiment shows a 13 cm^{-1} downshift (Table 5). Vibrational analyses of the DMABN ground state[38,39] show much more extensive vibrational coupling than we find for ABN, especially in the ring CC stretching and ring-substituent stretching (ν(ph-N) and ν(ph-CN)) modes. These are always hybridized with the ring CH bend motions and/or each other in ground state DMABN. The RCIS atomic displacements indicate similar complicated vibrational mixing in the LE state. Therefore, changes in the structure of DMABN cannot be inferred directly from the frequency shifts of the relevant modes. For example, the so-called ν(ph-N) mode is coupled substantially with the ring CH bending and CC stretching vibrations.[38,39] Consequently, the 13 cm^{-1} frequency downshift is not necessarily due to loosening of the ph-N bond in the LE state, but could result from the decrease of the phenyl ring force constants and the increase of the ring C−C lengths. The discrepancies between the calculated and experimental frequency observed here could be due to the crude level of the RCIS method, which is not sophisticated enough to take the vibrational hybridization character of DMABN fully into account. Comparison of experiment with calculated frequencies of much higher accuracy is essential to determine the structure. To our knowledge, there is as yet no adequate theoretical treatment for such a complicated excited state. However, as illustrated above, the RCIS method is reasonably successful in reproducing the experimental data for molecules that have less extensive vibrational coupling, such as ABN.

Molecular orbitals for ABN and DMABN related to the LE ← S_0 transition obtained from RCIS/6-31G(d) are shown in Figure 7. It is clear that the LE states with A″ symmetry in C_s are formed by a transition combining LUMO + 1 ← HOMO with ∼0.63 weight and LUMO ← HOMO − 1 with ∼0.32 weight. The promotion of an electron from the amino nitrogen lone pair to the ring antibonding π^* orbital can be clearly recognized in the first component. The second corresponds to an excitation from the ring bonding π orbital to ring antibonding π^* orbital and also leads to occupation of the C≡N antibonding π^* orbital. Analogous to aniline and many of its derivatives, the molecular orbital character of the LE states of ABN and DMABN are mainly $\pi\pi^*$, but with partial charge transfer mainly from the amino group to the phenyl ring and weakening of the C≡N bond. This is fully consistent with the frequency changes observed in our ps-TR[3] spectra and explains the calculated frequency and structural changes.

In summary, considering the similarities of ABN and DMABN fluorescence, transient absorption and TR[3] spectra and the general agreement of experiment with calculation, we propose a similar planar structure for the ABN and DMABN LE states.

5. Discussion

In the CASSCF study of ABN and DMABN by Dreyer et al.,[13,27] planar LE states similar to those suggested here and also pyramidal LE states were located by geometry optimizations. However, based mainly on comparison of calculated IR activities with experimental TRIR spectra,[10] pyramidal ABN and planar DMABN LE states have been suggested. The difference from our conclusion in the case of ABN originates from differences between our ps-TR[3] spectra and the TRIR spectrum[10] noted above. To our knowledge, the TRIR spectrum recorded in acetonitrile by Chudoba et al.[10] is the only previously published solution-phase vibrational spectrum of the LE state of ABN. In contrast to the substantial frequency shift of the C≡N, ring CC stretching and ν(ph-N) modes observed here (Figure 5a), they find only negligible frequency shifts and relatively small changes in IR band intensities upon formation of the LE state of ABN. The cause of these experimental differences is not known. Although one gas phase study by Berden et al.[33] seems to support the pyramidal LE state of ABN, our data is supported by a more recent gas phase rotationally resolved LIF and resonance two-photon ionization spectroscopy study by Lommatzsch et al.[21] and an LIF study of jet-cooled ABN by Gibson et al.[36] Ab inito RCIS calculations of the LE state of ABN by Lommatzsch et al.[21] give a planar structure similar to that proposed here.

Our spectra for the LE state of DMABN agree with our previous study[6] and also differ from the TRIR work.[10] The crucial C≡N and ν(ph-N) modes, which we observe clearly, are not present in the TRIR spectrum. In addition, in contrast to our observation of downshifts of the ring CC stretching modes (such as the 19a), they observed no shifts from ground-state frequencies.

In our previous work,[6] we tentatively attributed the ν(ph-N) mode to a strong band at 1423 cm^{-1} in the 615 nm spectrum (corresponding to the 1416 cm^{-1} band in Figure 5c). Considerng the d_6 isotopic shift and RCIS calculation, we now attribute the 1423 cm^{-1} band to a symmetric methyl deformation vibration. The mode dominated by ν(ph-N) is actually the band at 1357 cm^{-1}. The 1460 cm^{-1} LE state band provisionally assigned to a methyl vibration in the previous paper[6] is now found to be a mainly ring CC stretching mode (19a) according to the RCIS result. The shortening of the ph-N bond and planarity of the amino group suggested here is consistent with a microwave spectroscopy study of the LE state of DMABN by Kajimoto et al.[20] A structure with a 30° twist angle and a 0° inversion angle has been suggested for the LE state of DMABN by several authors.[20,21,24,25] However, as discussed by Kajimoto et al.[20] and Salgado et al.,[22] the simulated spectra were insensitive to the twist angle. This was well explained by a theoretical study by Roos et al.[32] and Gorse et al.[28] They found that the potential curve for the LE state in the gas phase is very flat from 0° to 30° along the twist angle coordinate, implying a very small torsional barrier up to 30° in the gas phase. However, by including solvent effects, Gorse et al.[28] showed that the shape of the LE state potential curve steepens as the twist angle is increased in both polar and nonpolar solvent, with a steeper slope in polar solvents. This causes the planar structure (0° twisting angle) to be the most stable conformation for the LE state in solution. This interpretation is in good agreement with our result, which is also supported by the semiempirical AM1-CI calculations of Schneider et al.[29] The twisted LE states of DMABN obtained using RCIS theory by Scholes et al.[26] and Lommatzsch et al.[21] are suspect, as the calculated transition moments do not agree with experiment.

Photoinduced changes in permanent electronic dipole moments reflect the degree of charge separation.[65,66] Dipole moment measurements by Schuddeboom et al. indicate increase of dipole moment from 6.6 to 8.0 D and from 6.6 to 9.9 D for ABN and DMABN, respectively, on going from the ground to LE state.[3] As the degree of localization of negative charge on the cyano group is the same for ABN and DMABN, as reflected by the same ∼30 cm^{-1} downshift of the C≡N frequency (section 4.3), and the two molecules have the same ground-state dipole moment, the larger dipole moment change in DMABN indicates greater charge separation between the amino and phenyl ring

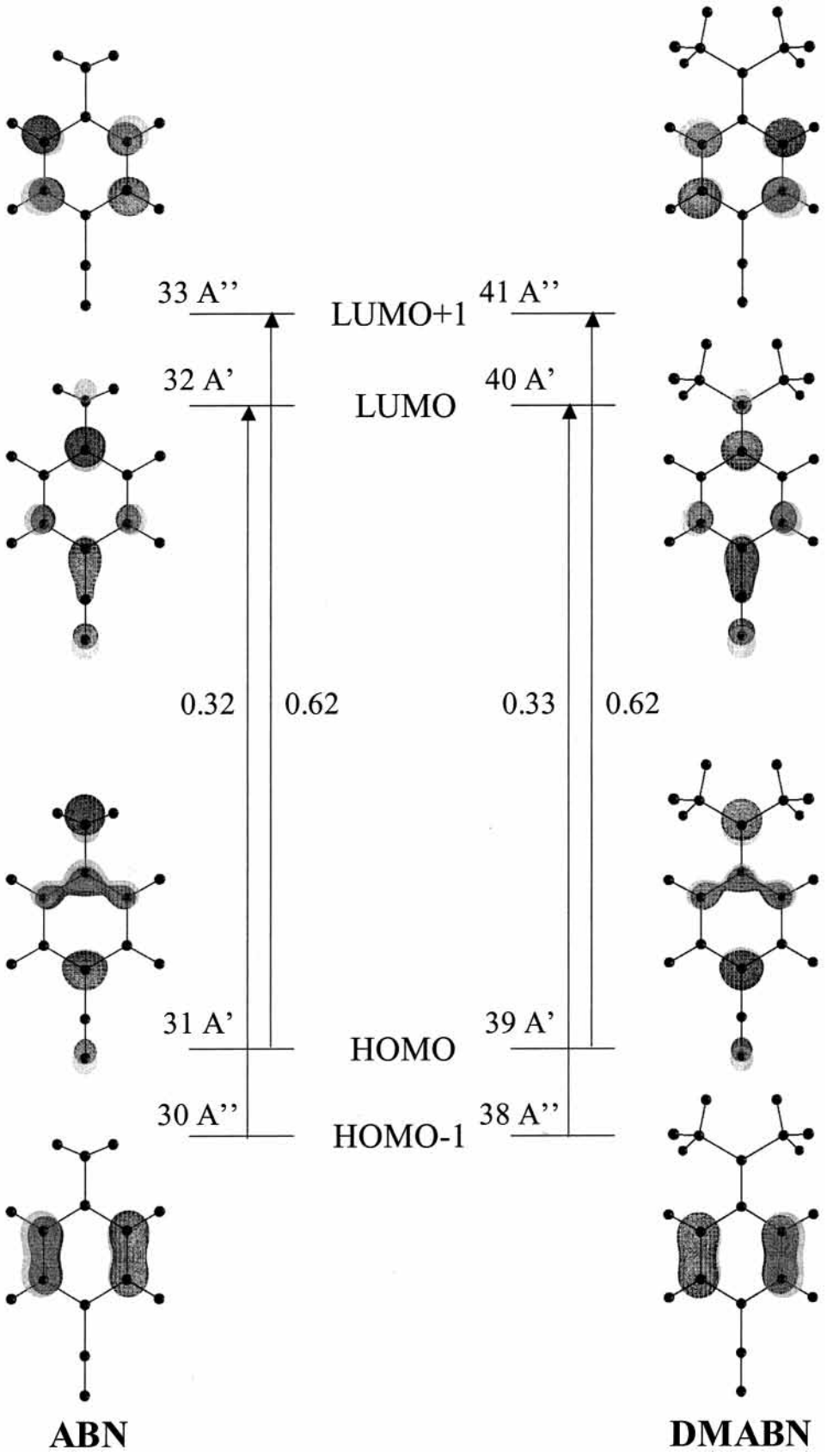

Figure 7. Calculated molecular orbitals of the LE states of ABN and DMABN.

in the LE state of DMABN than ABN. This implies increased localization of positive charge on the dimethylamino of DMABN than on the amino group of ABN, or in other words, greater degree of negative charge localized on the phenyl in the LE state of DMABN than ABN. This is clearly a consequence of more efficient transfer of charge from the amino nitrogen lone pair orbital to the π^* orbital of the ring in DMABN than ABN. This is well within expectation when considering the stronger electronic donor ability of the DMABN dimethylamino group relative to the ABN amino group.

Korter et al.[65] find that the dipole moment of aniline is ~150% larger in S_1 than in the ground state and suggest that the enhancement is due to more efficient electron donation resulting from a flattening of the pyramidal conformation of the amino group in S_1. This is consistent with the results presented here for ABN and DMABN. When the amino group and phenyl ring are coplanar, there is enhanced overlap of the nitrogen lone pair and ring π cloud, leading to efficient charge transfer and increased dipole moment of the LE state. Similar connections between changes in the charge distribution of the molecule and changes in its structure seem to be general for aromatic amines.[49−51,68,69]

We note that the planar conformation of the LE state of DMABN proposed here implies that the inversion coordinate of the dimethylamino group cannot serve as the ICT reaction coordinate and ICT rate-determining step, casting doubt on the PICT model.[4]

6. Conclusion

Picosecond-K-TR[3] and ps-TR[3] spectra of the LE state of ABN and DMABN have been obtained between 800 and 2400 cm^{-1} using different resonance Raman probe wavelengths, and ground state Raman and infrared spectra of ABN have been measured. We observe characteristic and reproducible frequency shifts from ground state values in several modes of both molecules. We note that these shifts were not observed in reported TRIR experiments. Combined with fluorescence and transient absorption measurements, our results strongly suggest a similar structure for the LE state of both ABN and DMABN. Based on the general agreement between experimental and ab initio calculated frequency shifts on going from the ground to LE state, planar structure has been proposed for the LE state of both the molecules. Excitation to the LE state flattens the molecules along the inversion coordination, expands the phenyl ring and shortens the ph-N bond. Partial charge-transfer character of the LE state is shown by a downshift of the ring CC stretching mode and an ~30 cm^{-1} frequency downshift of the C≡N stretching mode.

Acknowledgment. We are grateful to the EPSRC for financial support through grant GR/L84001. This work was carried out at the Central Laser Facility, CLRC Rutherford Appleton Laboratory. We thank Professor W. P. Griffith for his help in the conventional Raman measurements.

Appendix

Recursive Deconvolution. If D is a set of intensities, D_n, at regularly spaced frequencies denoted by the suffix, and the function to be deconvolved has values b_m at frequencies $k(m)$ in the regular set (but not necessarily evenly spaced), with $\Sigma b_m = 1$ and $k(0) = 0$, all other $k(m) > 0$, then D and the deconvolved spectrum, A, are related by

$$D_n = A_n b_0 + \Sigma_{m>0} A_{n-k(m)} b_m \qquad \text{(A1)}$$

Equation A1 is rearranged and solved for each A_n using recursion in Mathematica;[70] D must be defined as zero outside the measurement range.

References and Notes

(1) Lippert, E.; Rettig, W.; Bonacic-Koutecky, V.; Heisel, F.; Miehe, J. A. *Adv. Chem. Phys*. **1987**, *68*, 1.
(2) Rotkiewicz, K.; Grellmann, K. H.; Grabowski, Z. R. *Chem. Phys. Lett.* **1973**, *19*, 315.
(3) Schuddeboom, W.; Jonker, S. A.; Warman, J. M.; Leinhos, U.; Kuhnle, W.; Zachariasse, K. A. *J. Phys. Chem.* **1992**, *96*, 10809.
(4) Zachariasse, K. A.; Grobys, M.; Von der Haar, T.; Hebecker, A.; Ilchev, Y. V.; Jiang, Y.-B.; Morawski, O.; Kuhnle, W. *J. Photochem. Photobiol. A: Chem.* **1996**, *102*, 59.
(5) Sobolewski, A. L.; Sudholt, W.; Domcke, W. *Chem. Phys. Lett.* **1996**, *259*, 119.
(6) Kwok, W. M.; Ma, C.; Phillips, D.; Matousek, P.; Parker, A. W.; Towrie, M. *J. Phys. Chem. A* **2000**, *104*, 4188.
(7) Kwok, W. M.; Ma, C.; Matousek, P.; Parker, A. W.; Phillips, D.; Toner, W. T.; Towrie, M. *Chem. Phys. Lett*. **2000**, *322*, 395.
(8) Kwok, W. M.; Ma, C.; Matousek, P.; Parker, A. W.; Phillips, D.; Toner, W. T.; Towrie, M.; Umapathy, S. *J. Phys. Chem. A* **2001**, *105*, 984.
(9) Hashimoto, M.; Hamaguchi, H. *J. Phys. Chem.* **1995**, *99*, 7875.
(10) Chudoba, C.; Kummrow, A.; Dreyer, J.; Stenger, J.; Nibbering, E. T. J.; Elsaesser, T.; Zachariasse, K. A. *Chem. Phys. Lett*. **1999**, *309*, 357.
(11) Okamoto, H. *J. Phys. Chem. A* **2000**, *104*, 4182.
(12) Juchnovski, I.; Tsvetanov, C.; Panayotov, I. *Monatsh. Chem*. **1969**, *100*, 1980.
(13) Dreyer, J.; Kummrow, A. *J. Am. Chem. Soc*. **2000**, *122*, 2577.
(14) Kim, H. J.; Hynes, J. T. *J. Photochem. Photobiol. A: Chem*. **1997**, *105*, 337.
(15) Mennucci, B.; Toniolo, A.; Tomasi, J. *J. Am. Chem. Soc*. **2000**, *122*, 10621.
(16) Zachariasse, K. A. *Chem. Phys. Lett.* **2000**, *320*, 8.
(17) Parusel, A. B. J. *Chem. Phys. Lett.* **2001**, *340*, 531.
(18) Parusel, A. B. J. *Phys. Chem. Chem. Phys.* **2000**, *2*, 5545.
(19) Okamoto, H.; Inishi, H.; Nakamura, Y.; Kohtani, S.; Nakagaki, R. *J. Phys. Chem. A* **2001**, *105*, 4182.
(20) Kajimoto, O.; Yokoyama, H.; Ooshima, Y.; Endo, Y. *Chem. Phys. Lett*. **1991**, *179*, 455.
(21) Lommatzsch, U.; Brutschy, B. *Chem. Phys.* **1998**, *234*, 35.
(22) Salgado, F. P.; Herbich, J.; Kunst, A. G. M.; Rettschnick, R. P. H. *J. Phys. Chem. A* **1999**, *103*, 3184.
(23) Howells, D. B.; McCombie, J.; Palmer, T. F.; Simons, J. P.; Walters, A. *J. Chem. Soc., Faraday Trans.* **1992**, *88*, 2595.
(24) Warren, J. A.; Bernstein, E. R.; Seeman, J. I. *J. Chem. Phys.* **1988**, *88*, 871.
(25) Grassian, V. H.; Warren, J. A.; Bernstein, E. R.; Secor, H. V. *J. Chem. Phys.* **1989**, *90*, 3994.
(26) Scholes, G. D.; Phillips, D.; Gould, I. R. *Chem. Phys. Lett.* **1997**, *266*, 521.
(27) Kummrow, A.; Dreyer, J.; Chudoba, C.; Stenger, J.; Nibbering, E. T. J.; Elsaesser, T. *J. Chin. Chem. Soc.* **2000**, *47*, 721.
(28) Gorse, A.-D.; Pesquer, M. *J. Phys. Chem.* **1995**, *99*, 4039.
(29) Gedeck, P.; Schneider, S. *J. Photochem. Photobiol. A: Chem.* **1999**, *121*, 7.
(30) Lipinski, J.; Chojnacki, H.; Grabowski, Z. R.; Rotkiewicz, K. *Chem. Phys. Lett*. **1980**, *70*, 449.
(31) Leinhos, U.; Kuhnle, W.; Zachariasse, K. A. *J. Phys. Chem*. **1991**, *95*, 2013.
(32) Serrano-Andres, L.; Merchan, M.; Roos, B. O.; Lindh, R. *J. Am. Chem. Soc*. **1995**, *117*, 3189.
(33) Berden, G.; Rooy, J.; Meerts, W. L.; Zachariasse, K. A. *Chem. Phys. Lett*. **1997**, *278*, 373.
(34) Yu, H.; Joslin, E.; Crystall, B.; Smith, T.; Sinclair, W.; Phillips, D. *J. Phys. Chem.* **1993**, *97*, 8146.
(35) Yu, H.; Joslin, E.; Zain, S. M.; Rzepa, H.; Phillips, D. *Chem. Phys.* **1993**, *178*, 483.
(36) Gibson, E. M.; Jones, A. C.; Phillips, D. *Chem. Phys. Lett.* **1988**, *146*, 270.
(37) Heine, A.; Irmer, R. H.; Stalke, D.; Kuhnle, W.; Zachariasse, K. A. *Acta Crystallogr*. **1994**, *B50*, 363.
(38) Okamoto, H.; Inishi, H.; Nakamura, Y.; Kohtani, S.; Nakagaki, R. *Chem. Phys*. **2000**, *260*, 193.
(39) Kwok, W. M.; Gould, I.; Ma, C.; Puranik, M.; Umapathy, S.; Matousek, P.; Parker, A. W.; Phillips, D.; Toner, W. T.; Towrie, M. *Phys. Chem. Chem. Phys*. **2001**, *3*, 2424.
(40) Gates, P. N.; Steele, D.; Pearce, R. A. R.; Radcliffe, K. J. *Chem. Soc., Perkin Trans. 2* **1972**, 1607.
(41) Schneider, S.; Freunscht, P.; Brehm, G. *J. Raman Spectrosc*. **1997**, *28*, 305.
(42) Kumar, A. P.; Rao, G. R. *Spectrochim. Acta A* **1997**, *53*, 2049.
(43) Kumar, A. P.; Rao, G. R. *Spectrochim. Acta A* **1997**, *53*, 2023.
(44) Matousek, P.; Parker, A. W.; Taday, P. F.; Toner, W. T.; Towrie, M. *Opt. Commun*. **1996**, *127*, 307.
(45) Towrie, M.; Parker, A. W.; Shaikh, W.; Matousek, P. *Meas. Sci. Technol*. **1998**, *9*, 816.
(46) Frisch, M. J.; Trucks, G. W.; Schlegel, H. B.; Scuseria, G. E.; Robb, M. A.; Cheeseman, J. R.; Zakrzewski, V. G.; Montgomery, J. A., Jr.; Stratmann, R. E.; Burant, J. C.; Dapprich, S.; Millam, J. M.; Daniels, A. D.; Kudin, K. N.; Strain, M. C.; Farkas, O.; Tomasi, J.; Barone, V.; Cossi, M.; Cammi, R.; Mennucci, B.; Pomelli, C.; Adamo, C.; Clifford, S.; Ochterski, J.; Petersson, G. A.; Ayala, P. Y.; Cui, Q.; Morokuma, K.; Malick, D. K.; Rabuck, A. D.; Raghavachari, K.; Foresman, J. B.; Cioslowski, J.;

Ortiz, J. V.; Stefanov, B. B.; Liu, G.; Liashenko, A.; Piskorz, P.; Komaromi, I.; Gomperts, R.; Martin, R. L.; Fox, D. J.; Keith, T.; Al-Laham, M. A.; Peng, C. Y.; Nanayakkara, A.; Gonzalez, C.; Challacombe, M.; Gill, P. M. W.; Johnson, B. G.; Chen, W.; Wong, M. W.; Andres, J. L.; Head-Gordon, M.; Replogle, E. S.; Pople, J. A. *Gaussian 98*, revision A.7; Gaussian, Inc.: Pittsburgh, PA, 1998.

(47) Foresman, J. B.; Head-Gordon, M.; Pople, J. A.; Frisch, M. J. *J. Phys. Chem*. **1992**, *96*, 135.

(48) Rauhut, G.; Pulay, P. J. *Phys. Chem.* **1995**, *99*, 3093.

(49) Brouwer, A. M.; Wilbrandt, R. *J. Phys. Chem*. **1996**, *100*, 9678.

(50) Poizat, O.; Guichard, V.; Buntinx, G. *J. Chem. Phys*. **1989**, *90*, 4697.

(51) Guichard, V.; Bourkba, A.; Lautie, M.-F.; Poizat, O. *Spectrochim. Acta* **1989**, *45A*, 187.

(52) Cervellati, R.; Borgo, A. D.; Lister, D. G. *J. Mol. Struct*. **1982**, *78*, 161.

(53) Fukyo, M.; Hirotsu, K.; Higuchi, T. *Acta Crystallogr*. **1982**, *B38*, 640.

(54) Lister, D. G.; Tyler, J. K.; Hoeg, J. H.; Larsen, N. W. *Mol. Struct.* **1974**, *23*, 253.

(55) Mhin, B. J.; Park, B. H. *Chem. Phys. Lett.* **2000**, *325*, 61.

(56) Palafox, M. A.; Melendez, F. J. *J. Mol. Struct.* **1999**, *493*, 171.

(57) Yan, Y. J.; Mukamel, S. *J. Chem. Phys.* **1986**, *85*, 5908.

(58) Okada, T.; Uesugi, M.; Kohler, G.; Rechthaler, K.; Rotkiewicz, K.; Rettig, W.; Grabner, G. *Chem. Phys*. **1999**, *241*, 327.

(59) Ma, C.; Kwok, W. M.; Phillips, D.; Matousek, P.; Parker, A. W.; Towrie, M.; Toner, W. T. *CLF RAL. Ann. Rep.* **1999**−**2000**, 107.

(60) Clark, R. J. H.; Dines, T. J. *Angew. Chem., Int. Ed. Engl.* **1986**, *25*, 131.

(61) Ma, C.; Kwok, W. M.; Matousek, P.; Parker, A. W.; Phillips, D.; Toner, W. T.; Towrie, M. *J. Phys. Chem. A* **2001**, *105*, 4648.

(62) Varsanyi, G. Assignments for vibrational spectra of seven hundred benzene derivatives; Lang, L., Ed.; Adam Hilger: London, 1974; Vol. I.

(63) Kushto, G. P.; Jagodzinski, P. W. *Spectrochim. Acta, A* **1998**, *54*, 799.

(64) Rettig, W.; Wermuth, G.; Lippert, E. *Ber. Bunsen-Ges. Phys. Chem.* **1979**, *83*, 692.

(65) Korter, T. M.; Borst, D. R.; Butler, C. J.; Pratt, D. W. *J. Am. Chem. Soc*. **2001**, *123*, 96.

(66) Sinclair, W. E.; Pratt, D. W. *J. Chem. Phys*. **1996**, *105*, 7942 and references therein.

(67) Hollas, J. M.; Howson, M. R.; Ridley, T.; Halonen, L. *Chem. Phys. Lett*. **1983**, *98*, 253.

(68) Poizat, O.; Bourkba, A.; Buntinx, G.; Deffontaine, A.; Bridoux, M. *J. Chem. Phys.* **1987**, *87*, 6379.

(69) Chipman, D. M.; Sun, Q.; Tripathi, G. N. R. *J. Chem. Phys*. **1992**, *97*, 8073.

(70) Wolfram, S. *The Mathematica Book*, 3rd ed.; Wolfram Media and Cambridge University Press: Cambridge, 1996; Section 2.4.9.